Mapping Snow Sensor Usability in the Northern Hemisphere with Google Earth Engine

Victoria Ly

A thesis

submitted in partial fulfillment of the

requirements for the degree of

Master of Science in Civil Engineering

University of Washington

2020

Committee:

Jessica Lundquist

David Butman

Program Authorized to Offer Degree:

Civil and Environmental Engineering

University of Washington

Abstract

Mapping Snow Sensor Usability in the Northern Hemisphere with Google Earth Engine

Victoria Ly

Chair of the Supervisory Committee

Professor Jessica Lundquist

Civil and Environmental Engineering

Remote sensing provides a powerful tool for regularly observing seasonal snow properties across local, regional, and global spatial scales. Satellite Passive Microwave (PM) remote sensing provides a record of over 40 years of observation of snow properties like snow depth (SD) and snow water equivalent (SWE). PM sensor retrieval of snow can, however, have errors and uncertainty due to vegetation cover, snow depth, and snow wetness. While these limitations have been well-studied, they have not been organized to inform the application of snow products for other fields of research and/or resource management. This paper presents "Snow Sensor Usability Masks" (SSUM) that provide classifications where PM has demonstrated capability, potential capability, or no capability based on results from peer-reviewed publications. During the snow season (October to April), 33% of snow-covered areas in the Northern Hemisphere (excluding Greenland) have demonstrated capability with PM sensors. January has the greatest capability (42%) in the Northern Hemisphere, with February

following closely (37%). As a case study, evaluation near Quebec, Canada for the month of February illustrates that capability increased more when forest canopy thresholds increased than when SWE thresholds increased by order of magnitude of two. Our findings support the need for further development in methods to detect and quantify snow beneath forest and vegetation in PM radiance assimilation. This paper provides guidelines for applying PM snow products across the globe, as well as a framework for setting priorities for future PM data assimilation algorithm development and future snow field campaigns.

1. Introduction

The spatial extent and variability of seasonal snow is a crucial component of Earth's energy balance. Seasonal snow is the largest single component of the cryosphere, where the maximum average snow cover extent covers nearly 50% of the land cover area in the northern hemisphere (Robinson et al. 1993, Frei and Robinson 1999). For the past 30 years, spaceborne and airborne Passive Microwave (PM) sensors have been used to observe snow properties. PM has the unique benefit of penetrating clouds, providing a long record of observations, and measuring snow water equivalent (SWE). Satellite sensors, such as the Scanning Multichannel Microwave Radiometer (SMMR), the Special Sensor Microwave/Image (SSM/I), and the Advanced Microwave Scanning Radiometer Earth Observing System (AMSR-E) typically are scaled at ~25 km, and data assimilation algorithms scaled at ~5km (Takala et al. 2011, Pulliainen et al. 2006). PM derived datasets present valuable continuous, global scale observations of snow properties for long-term studies of earth's climate and energy balance.

However, the widespread use of PM sensors to estimate SWE is challenged by a number of factors. These include 1) the structure of the snowpack and presence of liquid water, 2) the spatial resolution, where subpixel heterogeneity in snow properties is not captured in large pixels, 3) vegetation, which impacts the measured microwave emissions from the snowpack and contributes additional emissivity from the canopy, and 4) the "saturation effect," where at a certain cut-off, additional snow accumulation has no evident effect on the PM brightness temperature (T_b) (Chang et al. 1987, Sturm et al, 1993, Kelly et al. 2003, Long et al. 2016). These all impact the nonlinear and multivariate relationship between T_b and SWE. For a review of these processes, the reader is referred to the background (Section 2) and referred to Table 1 for a summary of literature and cited parameters and thresholds.

The objective of this paper is to classify areas where PM sensors can feasibly retrieve snow measurements. Snow sensor usability has previously been characterized into three distinct classes: 1) demonstrated capability, 2) potential capability, and 3) no capability (NASA SnowEx Science Plan v1.7). The level of capability is defined by the limitations and range of cut-off values in the peer-reviewed literature . Demonstrated capability characterizes areas where the majority of literature agree that PM can retrieve a reliable signal. Potential capability characterizes areas where there is some disagreement in the cited literature about whether or not PM can retrieve a reliable signal. No capability characterizes areas where the literature agrees that PM cannot retrieve a signal due to limiting environmental factors. We focus our capability classifications on the ability of direct retrievals. Data assimilation techniques have the potential to increase capabilities, and the value of such improvements are addressed in the discussion.

To support analysis of global snow cover, we present a new data product, the Snow Sensor Usability Masks (SSUM), combining remote sensing observations that classifies snow-covered regions into three classes of feasibility. SSUM were produced at 25km to represent PM datasets that are operationally available and 5km to represent a case study of improved resolution. We use SSUM for the Northern Hemisphere to answer the following specific research questions:

1. What percentage of snow covered areas are classified with (a) demonstrated capability, (b) potential capability, and (c) no capability for PM sensors during the snow season (October-April)?

2. Which months have the highest percentage of demonstrated capability for PM?
3. How sensitive is our mapping algorithm to input dataset choices?
4. How much does the area mapped with capability change with increases in threshold ranges for forest cover and SWE?
5. How well does our map of capabilities match observations?

The paper is organized as follows: Section 2 summarizes the literature-defined limitations of PM. Section 3 contains descriptions of the study area, study period, and data. Section 3.3 describes the classification design in greater detail. Sections 4.1 and 4.2 show the baseline results of snow sensor usability, focusing only on non-mountainous areas. Section 4.3 addresses the sensitivity of our method to dataset choice. Section 4.4 evaluates the impact of changing forest and SWE threshold ranges. Section 4.5 evaluates baseline results compared with published observations. Section 5 interprets the significance of our findings. Section 5 also discusses the opportunities with PM algorithm development for complex terrain and mountains. Section 6 is devoted to the application of SSUM to water management and future work.

2. Background

2.1 Passive Microwave Sensor Theory

Passive microwave sensors detect radiance emitted from the earth's surface in bands between 110.7-89.0 GHz. The signal received by a PM sensor is typically represented as brightness temperature (T_b; in units of Kelvin) and is proportional to its physical temperature (T) in the microwave wavelength. In most retrieval algorithms, SWE retrievals are empirically derived, taking the difference in T_b between a lower and higher microwave frequency channel (Chang et al. 1976; Clifford 2010). For example, using a lower frequency (e.g., 18 GHz), a snowpack up to a depth of approximately 1 m is considered transparent, and the microwave emissions from Earth reach the radiometer. Using a second frequency (e.g., 37 GHz), the emissions from Earth are strongly scattered by snow, and the radiometer measures a lower T_b. The difference between the first and second frequencies marks the presence of snowpack, referred to as the 'spectral gradient' (Clifford 2010). SWE is derived by its empirically-derived linear relationship to the spectral gradient.

The capability of PM retrieval algorithms for accurate SWE observations is a function of factors that influence the emitted radiation reaching the radiometer, including 1) the physical structure of the snowpack, 2) the total snow mass, and 3) the radiation from the underlying ground. The following sections provide a brief summary of the literature used to determine the parameters and threshold ranges for empirical PM SWE retrievals (Summary in Table 1).

In general, forest radiative transfer models (Kim et al. 2019) and assimilating PM radiance measurements into a Land Surface Model (Durand and Margulis 2006, Durand and Margulis 2007) helps overcome many of the errors and limitations associated with empirically-based SWE retrieval algorithms. We refer to studies wherein radiance assimilation has demonstrated greater threshold ranges for SWE and tree canopy cover, respectively, and examine the impact of increasing these thresholds in Section 4.4.

2.2 Snow Composition (Liquid Water Content)

PM remote sensing of snow depends on the composition and structure of the snowpack. The crystalline structure of the snowpack impacts the T_b signal of snowpack. Larger snow grains decrease the total T_b signal received (Chang et. al 1987), redistributing upwelling radiation (Armstrong et al. 1993). The presence of liquid water changes the absorption and emittance of microwaves of the snowpack (Tedesco et al. 2006), decreasing volume scattering within the snowpack, limiting the radiation received by the radiometer (Dietz et al 2012). As much as 1% liquid water makes it impossible to determine SWE from PM remote sensing (Walker & Goodison 1993, Table 1).

2.3 Snow Depth

Greater overlying snow mass dampens the earth's microwave radiation that reaches the PM sensor (Chang et al. 1987). The obstacle with using the spectral gradient with retrieval algorithms is the "saturation effect" (Sturm et al. 1993, Kelly et al. 2003), where beyond a critical SWE value any further increase in SWE will not significantly change the T_b measured by a PM sensor. For retrieval algorithms that take the difference between a lower and higher frequency band, snow is "transparent" in the lower frequency channel, thus the critical SWE value matters for the higher frequency. Prior work has determined that PM can only retrieve SWE values between 10 mm and 200 mm for the 37 GHz frequency channel (Chang et al. 1987, Foster et al. 2005, Tedesco et al. 2006, Takala et al. 2011). The accuracy associated with the upper threshold of observable SWE is debatable depending on the site tested, and comparison between retrieval, modeled, and assimilated derivations, so we examine sensitivity to this threshold in Sections 6.2 and 6.3.

2.4 Forest cover

The impact of forest cover on PM SWE measurements depends on 1) pixel spatial resolution, 2) how much forest cover covers the pixel, and 3) the transmissivity of the forest cover, which depends on the tree species type. Forest cover complicates the T_b-SWE relationship because forest cover masks the emissions from snow-covered areas and also contributes its own emissions (Hall et al. 1982, Foster et al, 1991, Foster et al. 2005). Consequently, SWE retrievals derived from PM Tb observations in highly forested areas have been reported as having large errors and uncertainty (Chang et al., 1996; Hall, Foster, & Chang, 1982, Vander Jagt 2015). Fundamentally, the impact of forest cover on PM SWE retrieval will depend on whether we are considering a simple PM retrieval algorithm or more complicated radiance assimilation. For simple PM retrieval algorithms that involved two channel differencing, as described above, the upper cut-off for forest cover is 20% (Vuyovich et al. 2014, Foster et al. 2005). For radiance assimilation, the upper cut-off for forest cover is conservatively 50% (Durand et al. 2007, Li et al. 2017). Recent studies have supported the possibility that the upper cut-off for tree canopy cover can be up to 75% forest cover (Larue et al. 2018).

Table 1. Peer-reviewed literature defining threshold ranges for parameters that limit PM feasibility. Literature with a * indicates "baseline" choices for this study. Literature with ** indicates upper limits for testing threshold sensitivity to thresholds. Sensitivity tests are referred to in Table 4. threshold range choices for this study.

Parameter	Max. Threshold	Site tested	Citation	Journal	Method
Tree Canopy Cover Percentage	<15-30%	Western U.S.	Li et al. 2019	*IEEE Geoscience and Remote Sensing Letters*	Data assimilation
Tree Canopy Cover Percentage	< 20-30%	North America	*Vuyovich et al. 2014	*Water Resource Research*	Tb retrieval, Channel difference
Tree Canopy Cover Percentage	< 25%	Northern Quebec	Langlois et al. 2015	*IEEE Geoscience and Remote Sensing Letters*	Tb retrieval, Channel difference
Tree Canopy Cover Percentage	< 50%	North America	**Durand and Margulis 2007	*Journal of Geophysical Research Atmospheres,*	Data assimilation
Tree Canopy Cover Percentage	< 75%	Quebec (boreal forests)	**Larue et al. 2018	*Remote Sensing of Environment*	Data assimilation
Tree Canopy Cover Percentage	< 20-30%	Conterminous U.S.	*Foster et al. 2005	*Remote Sensing of Environment*	Tb retrieval, Channel difference
LAI	1.8 - 3.8 (LAI)	Colorado, U.S.	Vander Jagt et al. 2015	*Remote Sensing of Environment*	Tb retrieval, Channel difference
Snow Wetness	<1% LWC	Niwot Ridge, Colorado, U.S.	*Walker & Goodison 1993	*Annals of Glaciology*	--
Snow Water Equivalent (SWE)	< 150 mm	Northern Colorado and S. Wyoming, U.S. (CPLX-1)	*Tedesco et al. 2006	*IEEE Geoscience and Remote Sensing Letters*	Tb retrieval, Channel difference
Snow Water Equivalent (SWE)	< 150 mm	Northern Finland	*Kruopis et al. 1999	*IEEE Geoscience and Remote Sensing Letters*	Tb retrieval, Channel difference
Snow Water Equivalent (SWE)	150 mm +/- 40 mm	Canada (Northern Territories) , Finland, Eurasia (Russia, former Soviet Union)	*Takala et al 2011	*Remote Sensing of Environment*	Bayesian non-linear assimilation
Snow Water Equivalent (SWE)	200-300 mm	Sierra Nevada, US	**Kim et al. 2019	*Remote Sensing of Environment*	Data assimilation
Snow Depth (SD) Forest fraction	70 to 120 cm Max: 0.20	CLPX	Vander Jagt et al. 2013	*Remote Sensing of Environment*	Data assimilation
Terrain heterogeneity (slope)	< 2.5° (1.6-4.6°?)	Conterminous U.S.	Cho et al. 2020	*Water Resource Research*	Data assimilation

3. Data, Methods, and Study Areas.

3.1 Input Datasets

Five types of datasets were utilized in the classification schematic in this study (Table 2): snow cover extent data to determine snow presence; LST data as a proxy for snow melt and hence, liquid water presence in the snow; forest cover and leaf area index (LAI) to represent

fractional forest cover; SWE to represent snow depth/mass; and the Seasonal Mountain Snow Mask (SMSM) to represent complex terrain. Water bodies were masked out using the water body mask from Hansen et al. 2018.In-situ observations from LaRue et al. 2018 were used to evaluate the classifications. Terminology used in this paper is summarized in Table 2.

Table 2. Terminology and definitions referred to in this paper.

Term used	Definitions
Forest cover	Percentage of a pixel covered by forest
Limitations/ Parameters	Limitations to PM sensor retrieval, such as wet snow, forest cover, deep snow
Threshold range	The lower and upper limits of the parameters
Basic retrieval	Empirical PM SWE retrieval
Data assimilation	Radiance assimilation methods pushing the limitations of PM SWE retrieval
Baseline Threshold	Describes the following threshold ranges, using GlobSnow and Hansen et al. 2018 as input datasets for SWE and the forest cover limitations:
	"Demonstrated capability" is defined as LST < 0 °C, NDSI > 0.40, <20% forest cover, and <150mm SWE
	"Potential capability" is defined as LST < 0 °C, NDSI > 0.40, 20-30% forest cover, and <150mm SWE
	"No capability" is defined as LST < 0 °C, NDSI > 0.40, >30% forest cover and >150mm SWE

3.1.1 NDSI

MODIS Terra Daily Snow Cover (MOD10A1 v.6) was used to delineate the maximum area of snow cover extent. The MOD10_L2 algorithm was used to determine the Normalized Difference in Snow Index (NDSI) (Hall et al. 1995). Previous studies have determined that pixels with NDSI > 0.40 consistently represent snow cover (Hall et al. 1995, Dozier et al. 1989) in the United States (California, Montana, Alaska, and Minnesota) and Iceland. Clouds were excluded using the internal StateQA Bitmask cloud flags. Pixels with a NDSI > 0.40 were classified as having snow. Pixels with NDSI < 0.40 were considered snow free and were not included in the classifications or computations.

3.1.2 Snow Wetness (Liquid Water Content)

MODIS Aqua 8-day Land Surface Temperature (LST) was used as a proxy for snow wetness. Snow melt is indicated when LST reaches 0°C, which introduces liquid water into the snow pack. LST was converted from Kelvin to Celsius and then aggregated from daily to monthly mean of daytime LST.

3.1.3 Forest Cover

Forest cover was represented by the Hansen Global Forest Change v1.6 dataset (Hansen et al. 2018). This dataset is a time-series analysis of Landsat images capturing global forest extent and change from 2000-2012 at a spatial resolution of 30 m. Forest cover was defined as canopy closure for all vegetation taller than 5m in height for the year of 2000. The band used

was “tree_canopy_cover_2000”. This dataset was selected based on availability in GEE. Forest cover was resampled and averaged to a spatial resolution of 25 km for classifications.

In order to test the sensitivity of the usability classifications to the forest cover dataset, the MCD15A3H Version 6 MODIS Level 4, Combined Fraction of Photosynthetically Active Radiation, and Leaf Area Index 4-day composite product (Myneni et al. 2015; LAI) was compared to results using the Hansen et al. 2018 dataset (Section 4.3). The MCD15A3H algorithm selects the best pixel available from both the Terra and Aqua satellites from within the 4-day period. LAI is defined as one-half the total needle surface area per unit ground area in coniferous canopies and is a band in the data product (“Lai”), with an index value from 0-100. MODIS LAI was resampled from 500m to 25km and 5km for baseline and data assimilation results, respectively. Then LAI was aggregated from 4-day to monthly, and the mean of each pixel for the month was taken. The mean monthly LAI index value was used to represent mean forest cover percentage, where a value of 25 would be considered 25% forest canopy cover. Unlike the Hansen dataset, LAI changes with time of year as deciduous trees lose their foliage.

3.1.4 Snow Water Equivalent

GlobSnow was chosen as the baseline SWE input dataset because of its global availability and cited reliability for SWE estimation (Takala et al. 2011). GlobSnow snow water equivalent (SWE) uses a data assimilation scheme to integrate space-borne passive microwave sensors and ground-based weather stations from 1979 to 2012 over all non-mountainous areas of the Northern Hempisphere. SWE data derives from a number of PM sensors at different time periods, where Nimbus-7 SMMR, DMSP SSM/I and Aqua AMSR-E are the main data sources. SSM/I was used from 1987-2002, and AMSR-E was used from 2002-2010. GlobSnow monthly average SWE composites were reprojected from the EASE-Grid projection (Lambert Azimuthal) to WGS 84 to be imported into GEE. GlobSnow monthly average SWE v.2 has processing relics, represented as SWE values on coastlines. SWE relics were manually assigned no value.

To examine uncertainties related to using Globsnow as the baseline assumption of global SWE, baseline results were compared to results that used modeled SWE (Results Sections 5.4.1 and 5.5.1). Modeled SWE was drawn from Noah-MP version 3.6 (Noah-MP3.6, Niu et al., 2011; Yang et al., 2011). The NoahMP SWE data ranges from 2009-2017 and GlobSnow ranges from 1979-2016. NoahMP SWE data was averaged over 2009-2017 for the month of February. Two forcing datasets were used to drive the NoahMP model: 1) the Global Data Assimilation System (GDAS; Derber et al., 1991), and 2) the European Centre for Medium-Range Weather Forecasts (ECMWF; Molteni et al., 1996). Noah-MP SWE was selected to test against the baseline GlobSnow SWE because it represents a sophisticated and well-vetted model for snow data and is used operationally at major modeling centers (National Water Model). Noah-MP average SWE simulated using GDAS and ECMWF from 2009-2017, was reprojected to WGS 84, and resampled to a spatial resolution of 5km in Matlab. Noah-MP SWE simulations were then imported into GEE for further analyses.

3.1.5 Complex Terrain

For the baseline PM retrieval analysis, mountains were masked out using the Seasonal Snow Mountain Mask (Wrzesien et al 2019). For the PM sensitivity analysis, mountains were not masked to explore the role of complex terrain (Section 5). Slope was used as a proxy for

complex terrain to test the difference between using Wrzesien's mountain mask. The Shuttle Radar Topography Mission (SRTM) digital elevation data is used to calculate slope within GEE using the "terrain" function.

3.1.6 In-Situ Observations

Larue et al. (2018) investigated PM radiance assimilation for tree canopy cover, tree species type, and transitivity in northern Quebec. We plotted the location of the observations (latitude, longitude) with a 5km buffer. We used the reported fractional forest cover to categorize each in-situ point with demonstrated, potential, or no capability based on Sensitivity_Tree_Test_1 defined in Table 4. We compared our sensor usability classification for the month of February against Larue at al. finding whether PM worked or didn't work. (Results Section 4.6).

3.2 Pre-processing

Google Earth Engine (GEE) is an open-source, cloud-based platform for processing geospatial and tabular data at a planetary scale, with the facility to quickly share and edit code (Goerlick et al., 2017). GlobSnow, NoahMP GDAS, NoahMP ECWMF, and the Seasonal Mountain Snow Masks were reprojected to WGS 84 (EPSG: 4326) and imported into GEE. All other datasets (NDSI, LST, tree canopy cover, LAI) were available in the GEE library. Datasets for NDSI, LST, and LAI were each aggregated into mean monthly values for a total of 16 years (2002-2018), except for the Hansen et al. forest cover dataset, which describes only the year 2000. GlobSnow SWE was aggregated into mean monthly values for the entire available date range of 37 years (1979-2016). NoahMP SWE was aggregated for 8 years (2009-2017).

The resulting data product represents all land surface north of 20°N, except for Greenland. Ice and snow on top of ice sheets are beyond the scope of this paper. Results are first presented in 25km EASE grids to represent the spatial resolution of empirical PM SWE retrieval. Results are then presented in 5km to represent results if retrievals become available at a higher spatial resolution (Section 4.4). The temporal and spatial extents of datasets are summarized in Table 3.

Table 3. Datasets, spatial resolution, available temporal resolution. NDSI, LST, and LAI were processed from 2002-2018. Globsnow SWE was processed from 1979-2016. NoahMP SWE was processed from 2009-2017.

Parameter	Dataset	Spatial Resolution [km]	Units	Spatial coverage	Coordinate System	Temporal Resolution	Temporal coverage	Citation
Normalized Difference Snow Index (NDSI)	MODIS Terra Surface Reflectance 8-Day	0.50	Index	Global	Sinusoidal	Daily	March 3, 2000 - Present	Vermote, E. 2015
Snow Wetness	MODIS Land Surface Temperature (MOD11A1.006)	0.50	°F / °C	Global	Sinusoidal	8-day	Mar 5, 2000 - Present	Wan et al. 2015
Snow Water Equivalent (SWE)	GlobSnow average monthly SWE	25	mm	Global	Ease-Grid projection	Daily; Monthly	September 1979 - May 2016	Takala et al al. 2011

Snow Water Equivalent (SWE)	Noah-MP GDAS Noah-MP ECMWF	5	mm	North America	Gridded	Daily	2009 - 2017	Niu et al., 2011; Yang et al., 2011; Derber et al., 1991; Molteni et al., 1996
Tree Canopy Cover	Hansen Global Forest Change v1.6: Tree Canopy Cover 2000	0.03	Percentage	Global	WGS 84	Annual	2000	Hansen et al. 2013
Leaf Area Index (LAI)	MODIS Leaf Area Index (LAI)	0.5	Percentage	Global	Sinusoidal	4-day	July 4, 2002 - Present	Myneni et al. 2015
Slope	Shuttle Radar Topography Mission	0.03	Meters	Global	Gridded	Annual	2000	Farr et al. 2007

3.3 Classification Schematic

Input datasets were classified into three classes to represent geographic areas where PM sensors have "demonstrated capability," "potential capability," or "no capability" during the snow season (Fig. 2). Datasets within Google Earth Engine were processed over 2002-2018. Each input dataset (LST, NDSI, SWE, and forest cover) was averaged to a monthly time step (Appendix 1). Hence, each pixel represents the mean monthly value for October to April over the study time period (2002-2018). Classifications were based on a boolean algorithm, where the pixel was classified based on the input parameter and assigned threshold range set (Table 1). The resulting Snow Sensor Usability Masks were evaluated for the entire Northern Hemisphere domain using the baseline datasets and threshold ranges and then re-evaluated with variations on each of these to determine sensitivity to choice of input dataset or threshold value (see Table 1 and 2). For example, as the baseline, areas with LST < 0 °C, snow present as indicated by NDSI > 0.40, SWE < 150 mm, and forest cover cover < 20% were classified as "demonstrated capability." Areas with LST > 0 °C would be classified as "no capability," since this distinguishes areas with wet snow.

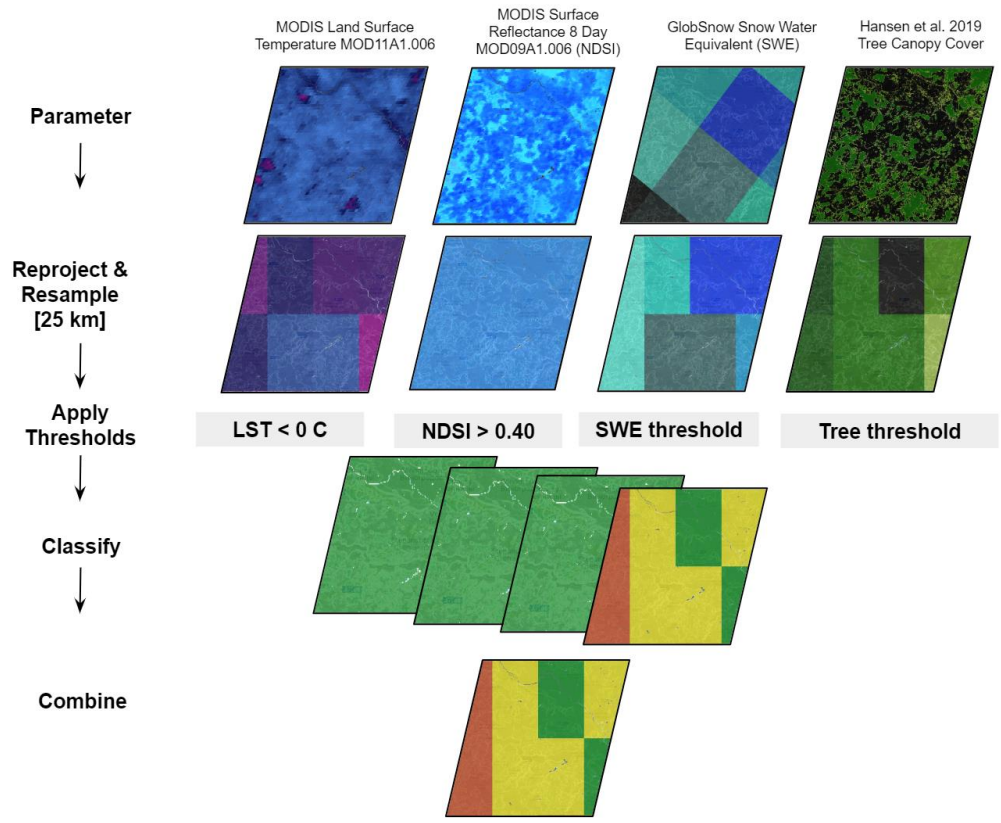

Fig. 1. Classification schematic within Google Earth Engine. Land surface temperature as a proxy for snow wetness, SWE, NDSI, and tree canopy cover were loaded and imported in Google Earth Engine. Datasets were resampled to 25km and reprojected to WGS84 (EPSG:4326). Threshold ranges (Appendix 4) were applied to each dataset. Classified layers were merged to make a final classification for each month.

3.2 Area Calculations

The area of each classification was calculated by taking the sum of each class for North America, Europe, East Asia, and Central Asia. Shapefiles used to define each of these continental areas were from the Large Scale International Boundary (LSIB) dataset (Office of the Geographer, US Department of State). The area [km^2] classified was computed for each month from October to April for each continental boundary. Total snow-covered area was computed for each month from October to April for each continental boundary, based on the proxy used for snow presence (NDSI > 0.40). The percent area of each class was calculated by taking the summed area of each class and dividing by the total non-mountainous, snow-covered area for each continent for each month and across the snow season.

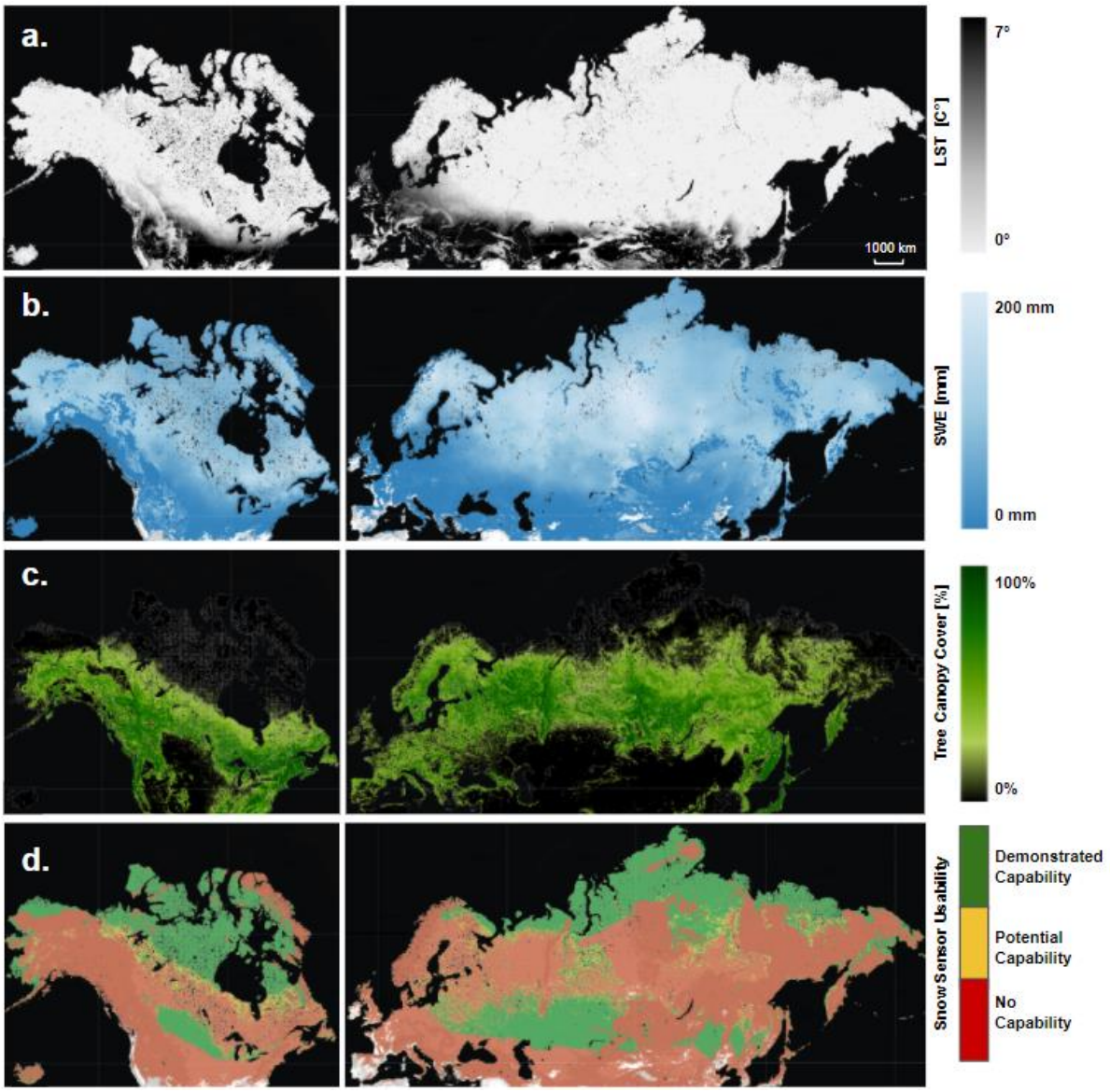

Fig. 2. Input datasets for baseline classifications of snow sensor usability. The following datasets were used to represent factors that limit the feasibility of PM retrieval of snow observations: (a) MODIS Land Surface Temperature as a proxy for locations where snow melt introduces liquid water in the snowpack, b) Hansen et al. 2018 tree canopy cover, (c) GlobSnow SWE. LST and SWE change for each month, Hansen et al. 2018 stays constant through seasons. (d) Snow Sensor Usability Masks (SSUM) for Passive Microwave sensors in the northern hemisphere for the month of January [25km]. Mountains and glaciers have been masked out. Europe and Asia are divided for summary statistics purposes.

3.3 Sensitivity analysis

3.3.1 Sensitivity analysis: Sub-set Study Areas

We selected two regions to address the sensitivity of the snow sensor usability masks to changes in datasets and threshold ranges: The NASA Cold Land Processes Experiment (CLPX) in Colorado, USA and the region near Quebec, Canada. The CLPX domain was selected because previous studies have tested microwave remote sensing for errors associated with snow depth

(Durand and Margulis 2009) and complex terrain (Kim et al. 2019). CLPX was a multi-sensor, multi-scale field campaign conducted in Colorado in 2002-2003 designed to use local-scale processes to expand to regional and global scales (Cline et al., 2003). This study focuses on the large regional study area (LRSA), which encompasses an area of 160,000 km^2 (Fig. 5). Secondly, Quebec was selected to compare results with previous studies that tested microwave remote sensing in areas with transitioning tree canopy cover and tree-snow interactions (La Rue et al. 2018).

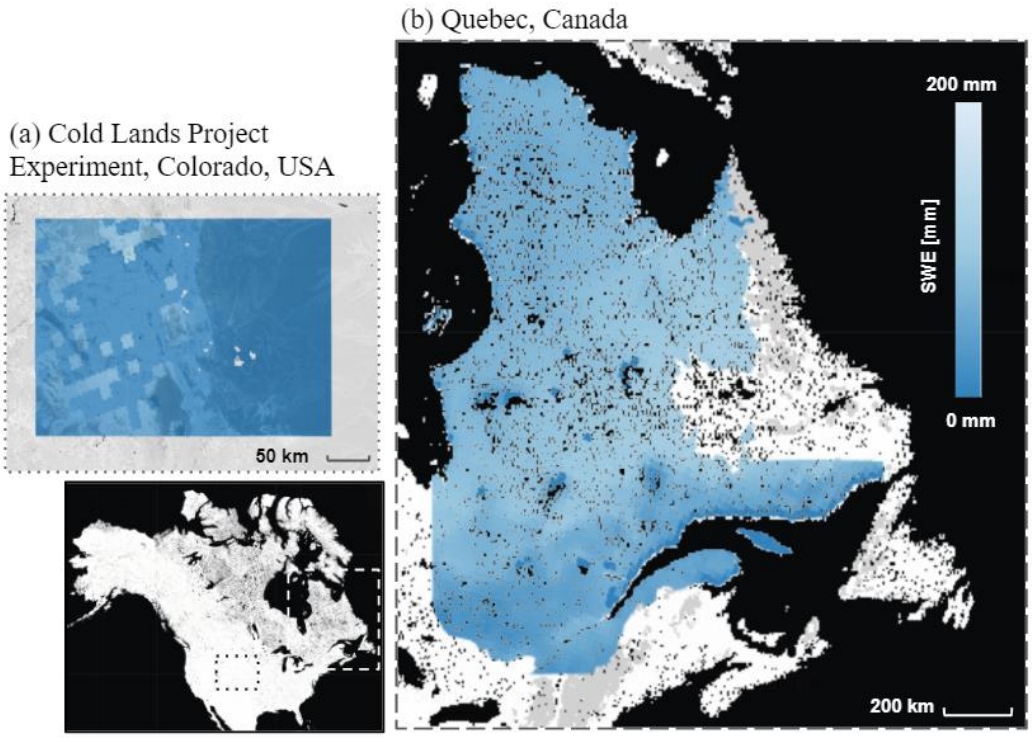

Figure 3. Sites selected for sensitivity analysis: (a) NASA Cold Lands Project Experiment (CLPX) in the Colorado Rockies and (b) Quebec, Canada. NoahMP ECMWF average SWE for the month of February (2009-2017) is shown here.

3.3.2 Sensitivity analysis: Area Calculations

The month of February was selected to evaluate the impact of changing data input for forest cover and SWE. For both the Quebec and CLPX domains (Fig. 3), Sensitivity tests were run to assess two datasets for trees and three datasets for SWE, each with low and high thresholds for forest and SWE cover (Table 4). The percentage area of sensor usability was calculated for each combination of forest and SWE datasets in GEE. The "ee.Image.pixelArea()" function was used to calculate the area with a certain pixel value. The ".reduceRegion()" function was used to sum the area in a defined region or interest.

Table 4. Key for Sensitivity tests over Quebec, Canada in the month of February. Tests evaluated changes in capability for changes in dataset and SWE and forest cover threshold ranges. The conditions of LST < 0 °C as a proxy for wet snow and NDSI > 0.40 as a proxy for snow presence are held constant. Range1, Range2, and Range3

indicate thresholds for SWE and forest cover with “demonstrated capability, ” “potential capability,” and “no capability,” respectively.

Test	Parameter	Dataset	Range1	Range2	Range3
Baseline	SWE	GlobSnow	< 150 mm	< 150 mm	> 150 mm
	Forest Cover	Hansen et al.	< 20%	20-30%	>30%
SensitivityTest_Dataset_1	SWE	NoahMP ECMWF	< 150 mm	< 150 mm	> 150 mm
	Forest Cover	Hansen et al.	< 20%	20-30%	>30%
SensitivityTest_Dataset_2	SWE	NoahMP GDAS	< 150 mm	< 150 mm	> 150 mm
	Forest Cover	Hansen et al.	< 20%	20-30%	>30%
SensitivityTest_Dataset_3	SWE	GlobSnow	< 150 mm	< 150 mm	> 150 mm
	Forest Cover	LAI	< 20%	20-30%	>30%
SensitivityTest_Dataset_4	SWE	NoahMP ECMWF	< 150 mm	< 150 mm	> 150 mm
	Forest Cover	LAI	< 20%	20-30%	>30%
SensitivityTest_Dataset_5	SWE	NoahMP GDAS	< 150 mm	< 150 mm	> 150 mm
	Forest Cover	LAI	< 20%	20-30%	>30%
SensitivtyTest_SWE_1	SWE	NoahMP ECMWF	< 200 mm	< 200 mm	> 200 mm
	Forest Cover	Hansen et al.	< 20%	20-30%	>30%
SensitivityTest_SWE_2	SWE	NoahMP GDAS	< 200 mm	< 200 mm	> 200 mm
	Forest Cover	Hansen et al.	< 20%	20-30%	>30%
SensitivityTest_Tree_1	SWE	GlobSnow	< 150 mm	< 150 mm	> 150 mm
	Forest Cover	Hansen et al.	< 50%	50-75%	>75%
SensitivityTest_Tree_2	SWE	GlobSnow	< 150 mm	< 150 mm	> 150 mm
	Forest Cover	LAI	< 50%	50-75%	>75%
SensitivityTest_Tree_3	SWE	NoahMP ECMWF	< 150 mm	< 150 mm	> 150 mm
	Forest Cover	LAI	< 50%	50-75%	>75%
SensitivityTest_Tree_4	SWE	NoahMP GDAS	< 150 mm	< 150 mm	> 150 mm
	Forest Cover	LAI	< 50%	50-75%	>75%

4. Results

4.1 Spatial analysis by continent

Snow Sensor Usability Masks were first assessed using baseline thresholds (Table 4).

The sensor usability areas classified by percentage for Eurasia and North America are summarized in Fig. 4a. PM sensors can feasibly retrieve snow information for approximately 33% of the non-mountainous, snow-covered area in the northern hemisphere snow season (55.9 x 10^6 km^2). PM sensors have no capability for 61% of the non-mountainous, snow-covered area in the northern hemisphere from October to April (103.4 x 10^6 km^2). 7% of the non-mountainous, snow-covered area in the northern hemisphere was classified with potential capability (12.7 x 10^6 km^2). The baseline SSUM product is available on Google Earth Engine (https://code.earthengine.google.com/?asset=users/victorialy/SSUM) and are available for download from Zenodo (Ly et al. 2020)

Continent	Non-mountainous, snow-covered area [km^2]	No Capability [km^2]	Potential Capability [km^2]	Demonstrated Capability [km^2]	No Capability [%]	Potential Capability [%]	Demonstrated Capability [%]
Eurasia	112,601,918	68,683,767	6,176,646	36,616,052	40	3	21
North America	57,807,830	34,815,587	6,582,084	19,341,568	20	4	11
Northern Hemisphere	170,409,748	103,499,353	12,758,730	55,957,620	60	7	33

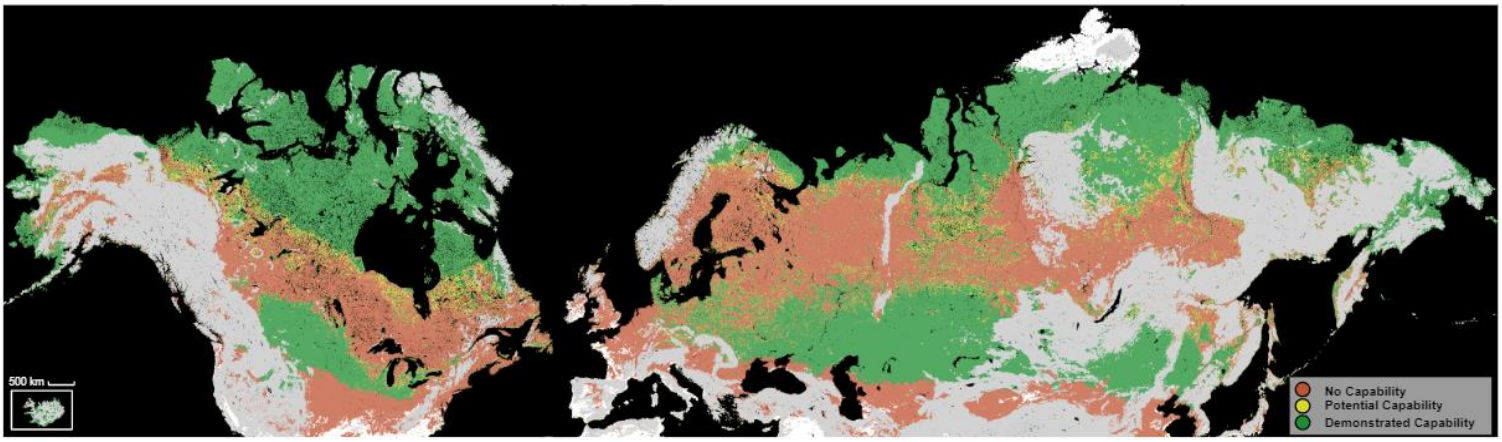

Figure 4. (a) Above: Table 3. Total area classified as demonstrated, potential, and no capability by continent (October - March). Percentages are expressed as the area of each classification divided by the total non-mountainous, snow covered area in the northern hemisphere. **(b) Below**: **Snow Sensor Usability Mask (SSUM) of the Northern Hemisphere for the month of February using the baseline threshold as defined in Table 4.** Mountains are masked using the Snow Mountain Masks (Wrzsien et al. 2019).

For illustrative purposes, we examine January/February because it represents the maximum global snow extent and aligns with the dates for major snow field campaigns (e.g. NASA SnowEx, NASA CLPX). In North America, PM sensors can feasibly retrieve snow characteristics in the Great Plains in the United States (eastern Montana, North Dakota, South Dakota, and Iowa) and southern Saskatchewan and Alberta provinces in Canada. Additionally,

PM sensors have demonstrated capability in northern Quebec and the Northwest Territories of Canada in Nunavut, and northern Alaska. In Europe, the areas with greatest potential capability include Germany, Poland, Belarus, and Lithuania. Generally, PM sensors could feasibly retrieve observations for most of northern Russia, Ukraine, Kazakhstan, Mongolia, and northern China.

4.2 Temporal analysis by month

Globally, December, January, and February have the greatest area with demonstrated capability (Fig. 5). January has the greatest area with demonstrated capability (43%), with February (37%) close behind (Figure 3a). April has the least area with demonstrated capability (23%), followed by March (24%). The temporal patterns are primarily driven by LST during the snow accumulation phase, where the snow is not melting. SWE increases throughout the season, but is not as much of a driver because the dataset used is capped at 150mm.

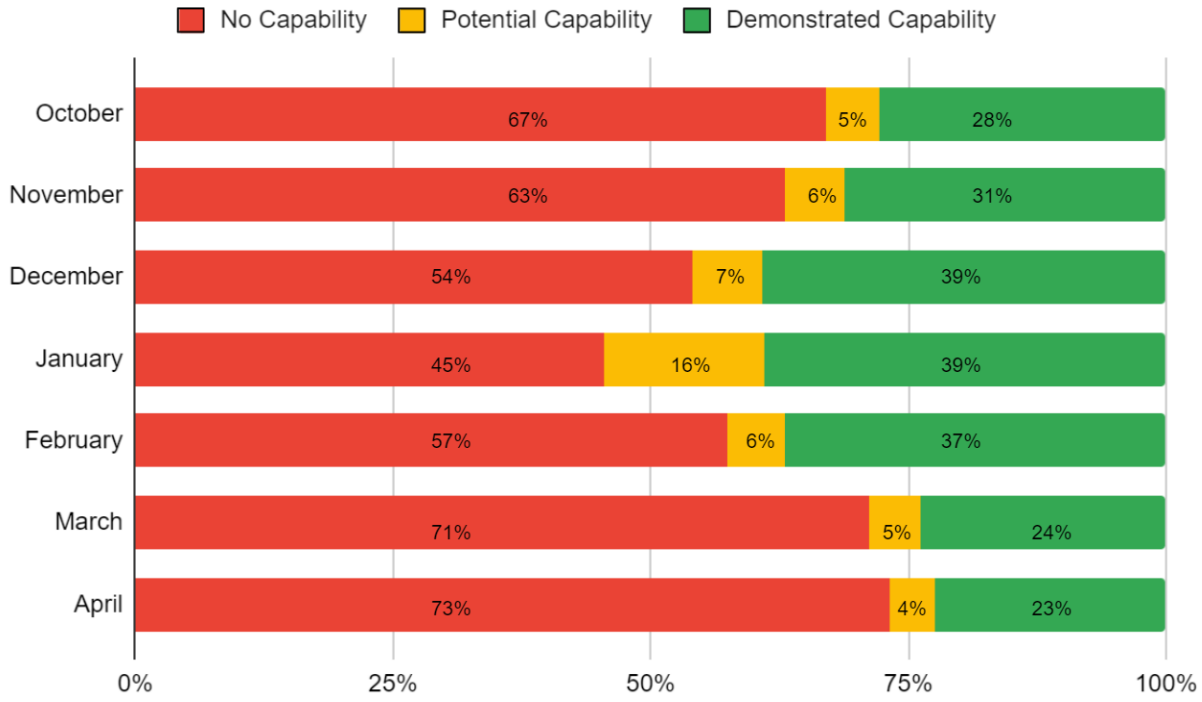

Figure 5. Histogram of area [km^2] classified with demonstrated capability, potential capability, and no capability in the northern hemisphere over the snow season from October to April. Area calculations were based on baseline thresholds as defined in Table 4.

4.3 Sensitivity of results to input datasets

4.3.1 Sensitivity to SWE dataset

Three input datasets of mean February SWE were tested in Quebec to compare sensitivity to dataset choice (Table 4). As illustrated with cumulative density functions of SWE (Fig. 6e), NoahMP GDAS consistently reported the deepest snow (max 534 mm SWE), NoahMP ECMWF reported moderately deep snow (max 442 mm SWE), and Globsnow reported the shallowest snow (max 167 mm SWE). NoahMP ECMWF has the greatest range of mean SWE values for the month of February. The snow sensor usability classifications arising from the three different

SWE datasets spatially differed (Fig. 6a-d). The greatest difference in total area with demonstrated capability was between GlobSnow and NoahMP GDAS (20% more feasible area with GlobSnow). The area classified with the least difference in demonstrated capability was GlobSnow and NoahMP ECMWF (7% more feasible area with GlobSnow).

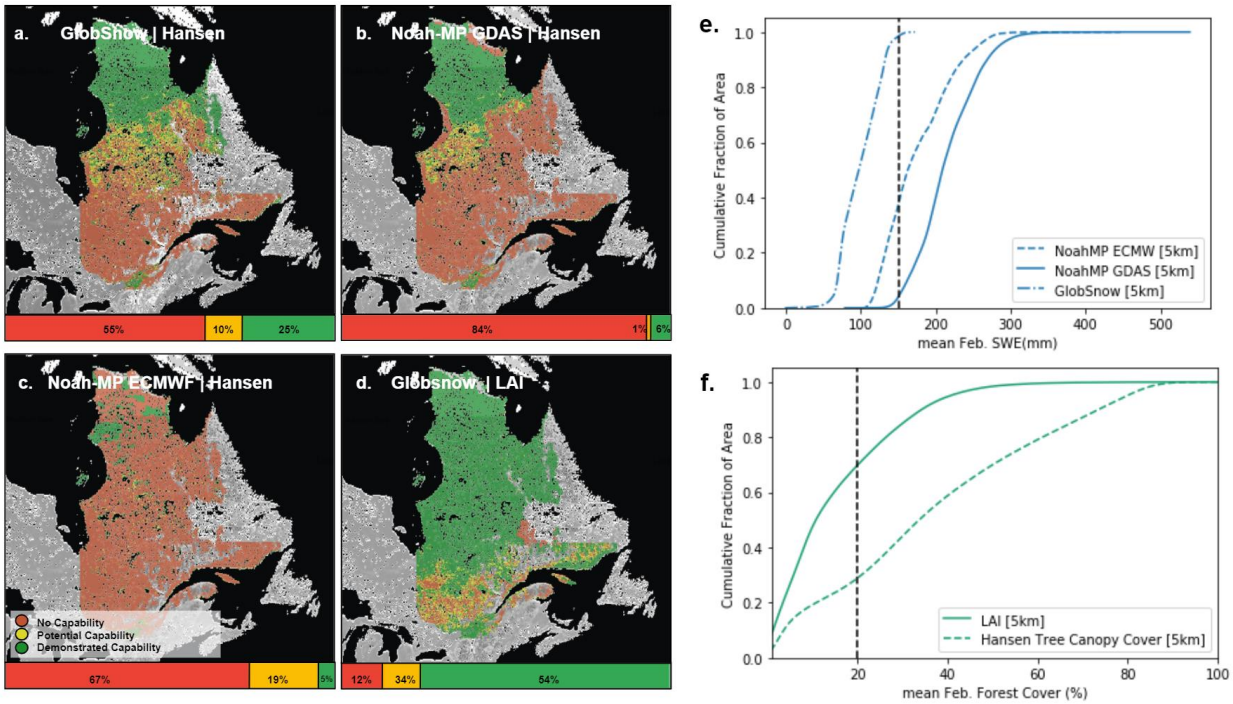

Fig. 6. Changed capability using different SWE and Tree Canopy Cover datasets.

(a) GlobSnow SWE, (b) NoahMP GDAS, and (c) NoahMP ECMWF with the Hansen et al. 2018 tree canopy cover dataset were used to test the sensitivity of classifications to the SWE input dataset in Quebec for February. (d) GlobSnow and mean LAI were used to test the sensitivity of classifications to tree canopy cover dataset in Quebec. Histograms below the respective maps in 6a-d illustrate the total classified area for Quebec for February. (e) Cumulative distribution functions for SWE datasets in Quebec for February. (f) Cumulative distribution functions for tree canopy datasets in Quebec for February.

4.3.2 Sensitivity of results to forest cover dataset

Results to changes in forest cover dataset are summarized in Table 5. The greatest difference in total area with demonstrated capability was between Hansen et al. 2018 and the LAI dataset with GlobSnow as the constant SWE input (29% more feasible area with LAI). The difference between Hansen et al. 2018 and the LAI dataset with NoahMP ECMWF as the constant SWE input was also considerable (15% more feasible area with LAI).

Table 5. Area classification calculations for Quebec, Canada in the month of February. SWE has a strict threshold (demonstrated or no capability, with no potential capability zone), whereas the tree canopy has a "potential capability" zone. Sensitivity tests for tree thresholds are noted with a *. See Table 2 for specific threshold ranges defined for each test.

Test ID Name	SWE dataset [5km]	Tree dataset [5km]	SWE threshold	Tree canopy cover threshold	Area Classified - Demonstrated Capability	Area Classified - Potential Capability	Area Classified - No Capability	% Difference in Demonstrated Capability from baseline
Baseline	GlobSnow	Hansen et al.	150 mm	20-30%	25%	10%	55%	*baseline*
Sensitivity_Dataset_1	NoahMP ECMWF	Hansen et al.	150 mm	20-30%	19%	5%	67%	-7%
Sensitivity_Dataset_2	NoahMP GDAS	Hansen et al.	150 mm	20-30%	6%	1%	84%	-20%
Sensitivity_Dataset_3	GlobSnow	LAI	150 mm	20-30%	54%	34%	12%	29%
Sensitivity_Dataset_4	NoahMP ECMWF	LAI	150 mm	20-30%	34%	3%	54%	8%
Sensitivity_Dataset_5	NoahMP GDAS	LAI	150 mm	20-30%	9%	1%	81%	-16%
Sensitivty_SWE_1	NoahMP ECMWF	Hansen et al.	200 mm	20-30%	23%	9%	59%	-3%
Sensitivity_SWE_2	NoahMP GDAS	Hansen et al.	200 mm	20-30%	17%	4%	70%	-9%
*Sensitivity_Tree_1	GlobSnow	Hansen et al.	150 mm	50-75%	54%	19%	18%	28%
*Sensitivity_Tree_2	GlobSnow	LAI	150 mm	50-75%	97%	1%	1%	72%
*Sensitivity_Tree_3	NoahMP ECMWF	LAI	150 mm	50-75%	10%	0%	80%	-15%
*Sensitivity_Tree_4	NoahMP GDAS	LAI	150 mm	50-75%	38%	0%	52%	13%

4.4 Sensitivity of results to threshold cutoffs

*4.4.1 Sensitivity of results to set SWE threshold **cutoffs***

Cumulative distribution functions (Fig. 6e) illustrate how increasing the threshold of the deepest observable SWE changes the observable area as a function of dataset. For example, GlobSnow reports that 100% of the region has SWE values less than or equal to 150 mm, so increasing the threshold when using this dataset has no effect in this region. However, Noah-MP-GDAS reports about 25% of the area deeper than 150 mm, and Noah-MP-ECMWF reports about 40% deeper than this threshold. Thus some subset of these areas (those not blocked by trees or snow wetness) are sensitive to the SWE threshold.

Increasing the upper SWE threshold from 150mm to 250mm was tested for North America and Quebec, Canada for the month of February. For North America, demonstrated capability area increased by 3% using Noah-MP ECMWF and 5% using Noah-MP GDAS.

Potential capability area increased minimally (1% for Noah-MP ECMWF and Noah-MP GDAS). For Quebec, demonstrated capability area increased by 7% using Noah-MP ECMWF and 17% using Noah-MP GDAS. Potential capability area increased minimally (6% for Noah-MP ECMWF and 8% for Noah-MP GDAS). Under our classification scheme, potential capability is set by forest cover because forest cover has a middle ground; whereas changes in the SWE threshold will change the area classified with demonstrated capability or no capability. In Quebec, increasing the upper SWE threshold means that there are areas where SWE can be sensed.

*4.4.2 Sensitivity of results to forest cover threshold **cutoffs***

Cumulative distribution functions (Fig. 6f) illustrate how increasing the threshold of dense observable forest cover changes the observable area as a function of dataset. For example, the LAI dataset reports 100% of the region has forest cover values less than or equal to 50%. However, the Hansen et al. (2018) dataset reports about 40% of the region has forest cover less than or equal to 50%. For the Quebec region only (Fig. 6d), the area with demonstrated capability increased 19% with the LAI dataset instead of the Hansen et al. (2018) dataset. The area with potential capability increased 24% with the LAI dataset over the Hansen et al. (2018) dataset.

Increasing the upper forest canopy threshold range from 20-30% to 50-75% was tested for North America and Quebec, Canada for the month of February. For North America, results showed demonstrated capability increased a similar magnitude with the LAI dataset or Hansen et al. (2018) dataset (11% and 12%, respectively). Potential capability increased similarly with both datasets, as well (3% and 6%, respectively). For Quebec, using the LAI dataset had a greater impact on classified demonstrated capability than the Hansen et al. (2018) dataset (33% increase with LAI, 19% increase with Hansen et al.). Additionally, increasing the allowable forest threshold had increased potential capability (33% with LAI, 9% with the Hansen et al. 2018 dataset).

4.5 Comparison of Classifications to Cited Literature

The Snow Sensor Usability Maps (SSUM) presented here provide a way for water resource managers and researchers to check if PM-derived snow data products can feasibly work in their region of interest. Larue et al. (2018) investigated the contribution of forest cover to PM signals in boreal forests in Quebec by experimenting with three different data assimilation schemes and varying forest cover. They found that the accuracy of SWE simulations (by way of T_B assimilation) is achieved when forest cover is below 75%. As a quick evaluation of our baseline snow sensor usability classifications, we plotted the sites from Larue et al. (2018) by forest cover and classified each site based on "SensitivityTest_Tree_1" accurate SWE observations with forest cover below 75%. We found that 6 out of 10 sites from Larue et al. (2018) matched our baseline classification (Fig. 7).

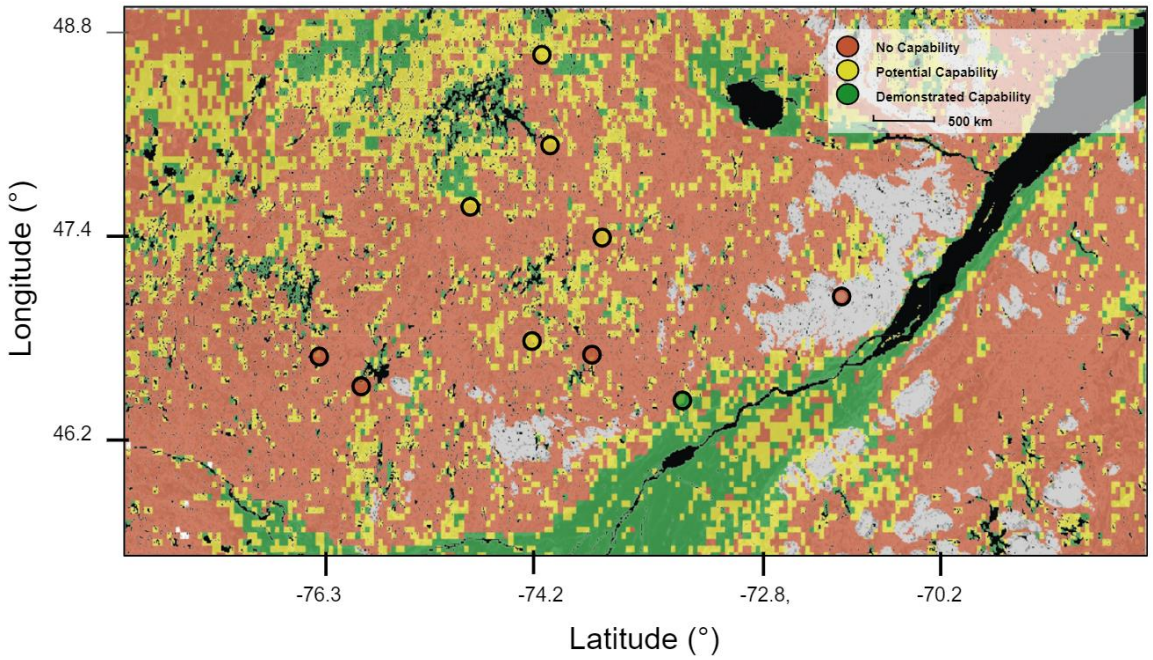

Fig 7. Comparison of sensor usability classifications to previous studies in Quebec. GlobSnow and Hansen et al. 2019 are used as SWE and fractional tree cover inputs, respectively, in the classification. Sites from LaRue et al. 2018 are overlaid. Capability is defined by the thresholds listed for "SensitivityTest_Tree_1" in Table 4.

5. Discussion

The goal of this paper is to clearly illustrate where in the world PM can accurately retrieve SWE observations. Secondly, this paper serves to provide a proof of concept for determining the most optimal areas and times for guidelines for applying snow products, future satellite mission planning, and setting priorities for future PM data assimilation algorithm development. We presented and evaluated Snow Sensor Usability Masks, which identified 33% of the snow-covered Northern Hemisphere as having demonstrated capability during the snow season. We highlight January and February since these months have the highest percentage of demonstrated capability for PM in the Northern Hemisphere.

Thus far, our focus has been on the capability of basic PM retrieval algorithms, such as can be readily accessed for global datasets, like AMSR-E (Chang and Rango 2000), GlobSnow (Takala et al. 2011), and the Canadian Sea Ice and Snow Evolution Network (CanSISE; Mudryk et al. 2015). These algorithms have known limitations due to liquid water content, forest cover, snow water equivalent, and complex terrain. Various approaches using radiance assimilation (Table 1 and 4) suggest that there is potential to push all of these limitations, with the exception of liquid water content. Here we discuss how our mapping algorithm identifies how potential improvements in each limitation are likely to increase the area of PM capability.

In Section 4.4, we found that constraints due to forest cover were more limiting than constraints due to snow depth (or SWE). This was particularly true for areas near the boreal

forest. To compare the constraints of forest cover and snow depth in a boreal forest region, we compared two cases for February in Quebec: increasing the forest cover limitation and increasing the SWE limitation. The total area with demonstrated and potential capability increases by nearly half of the area (48%) in Quebec with increasing the forest cover cut-off, whereas the total area with demonstrated and potential capability increases by less than a quarter of the area (13-26%) in Quebec with increasing the SWE cut-off. Therefore, we recommend prioritizing the development of assimilation techniques to detect snow beneath forest cover above assimilation work to quantify deeper snow.

We found that sensor capability differed with different datasets representing deep snow and forest cover (Section 4.3). Future work could be invested in testing current and additional datasets. For SWE datasets, it would be beneficial to sub-set the GlobSnow SWE dataset to overlap the exact time range with the NoahMP datasets (2009-2016) to test how much variability is due to the model as opposed to the time-period investigated. For forest cover, it would be beneficial to test scaling issues with LAI and forest canopy. Here, LAI as an index from 0-100 was treated as the forest cover percentage. Previous studies like Varhola et al. 2013 have compared vegetative metrics, including LAI and tree canopy cover. Next steps would be to investigate the relationship between LAI and forest canopy for pine needles, in order to confirm the relationship between datasets. Additionally, we recommend evaluating the impact of different classifications for forest cover using fractional tree cover with NASA Making Earth System Data Records for Use in Research Environments (MEaSUREs; Hansen & Song 2018) or a more categorical dataset like, land cover type (Channan et al. 2014). Identifying the limitations due to snow type could provide some insight with using Seasonal snow classes (Sturm et al. 2010).

Mountains have been noted as problematic due to steep slopes (Kim et al. 2019) and sensor resolution (Long et al. 2016), but they also have a considerable amount of forest cover and deep snow. Mountains comprise ~25% of the continental land area and ~27% of the total snow-covered area in CONUS (Wrzesien et al. 2019). If we were to overcome the slope and resolution issues, how much more area would be visible in mountains if forest cover and deep snow remained problematic? To address this, we examine the CLPX site in Colorado (Fig. 7b). Total area with demonstrated capability increases approximately 27% over the CLPX domain when mountains are not masked out.

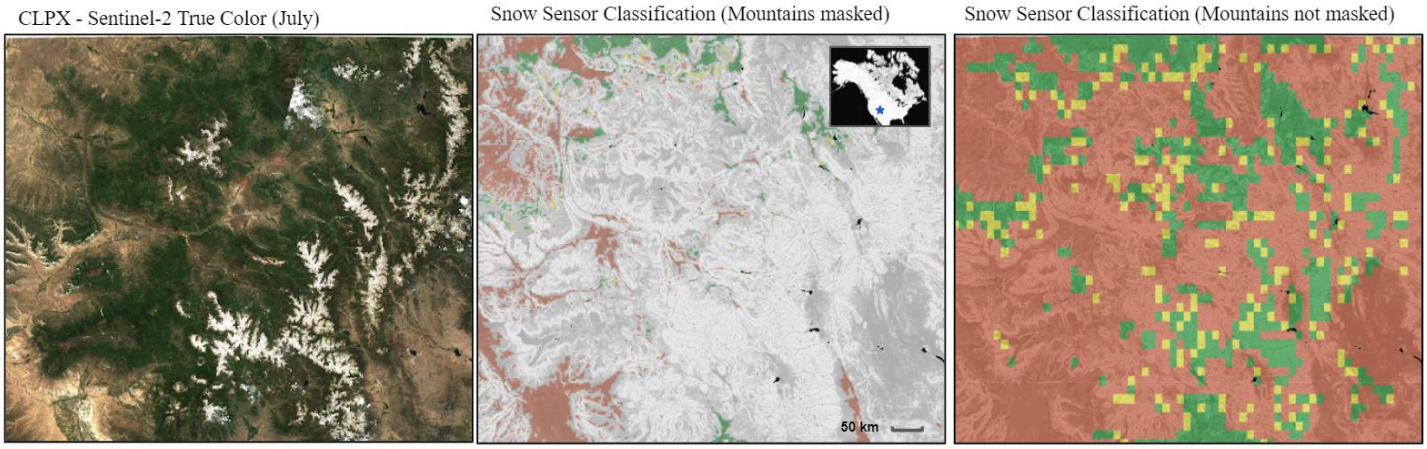

Fig. 7. Feasibility in heterogeneous terrain over CLPX. Classifications used LAI at a 20-30% threshold as the tree canopy cover input and NoahMP ECMWF as the SWE input, with the following constraints on terrain: a) All mountains masked out using SMSM (Wrzesien et al. 2019) and b) All mountains not masked out.

One application of the Snow Sensor Usability Masks is to provide a framework to determine the usability and limitations of other sensors used to observe snow properties. Here we have applied this framework to passive microwave sensors, but maps of capability vs. no capability could be applied globally to other sensor types as well (see Appendix 5 for examples of other sensors considered by the NASA SnowEx Science Plan. By extending the framework of this study to multiple sensor types, considering each of their limitations, SSUMs could become a strategic tool for assessing the application of multiple snow products, designing field campaigns, and prioritizing algorithm development for PM and other other snow sensors.

6. Conclusion

In this study, we present the first Snow Sensor Usability Masks (SSUM) that classify the Northern Hemisphere into three classes, where PM sensors have demonstrated capability, potential capability, and no capability to retrieve snow properties. Our results suggest that in February, 37% of Northern Hemisphere snow covered areas have snow water equivalent that can be accurately determined using PM remote sensing. Other areas have one or more sensor limitations impeding adequate retrieval, such as liquid water present, too much forest cover, or too much snow. Prior to this study, PM SWE values have been provided uniformly over snow covered areas, without clarification of where they provide useful information. This has led to confusion and sometimes misuse of information. The masks developed here provide a readily accessible overlay to allow resource managers and scientists to determine whether PM SWE provides capability for their area, time period, and questions of interest. Rather than the dichotomy of PM either being used in places with bad information or being excluded everywhere

due to a lack of trust, the maps provide clear guidelines for when and where the information can be applied.

Sensitivity tests illustrate that increasing the upper limits of the forest cover threshold range results in greater increases to the area with demonstrated capability than does increasing the upper limits of the SWE threshold range. Thus, future research should prioritize increasing retrieval capabilities under canopy cover. Emerging PM data assimilation approaches (Vander Jagt et al. 2015, Langlois et al. 2011) show potential here.. The boreal forest in North America and Eurasia present an opportunity for future PM snow modeling, algorithm development, and ground measurement experiments. This study also provides a proof of concept of classifying sensor usability at a large spatial scale. Furthermore, this work provides a platform for future work to identify limiting parameters and thresholds for other sensors to support a larger mission of prioritizing methods and instruments for global snow monitoring.

Acknowledgements

This material is based upon work supported by the National Science Foundation Graduate Research Fellowship Program under We also Grant No. DGE-1762114. We wish to thank Michael Durand from the University of Ohio, Carrie Vuyoich, and Melissa Wrzesien from the NASA Goddard Space Center for their collaboration. The author thanks Vaughn Iverson and Scott Henderson from the UW eScience Institute for their assistance in developing the pre-processing workflow and code; and Maura Rowell for her help in data processing during the 2019 UW GeoHack Week. The author sends gratitude to the UW Hydrology Department, especially to Steven Pestana and Michelle Hu for their support and patience. The author would also like to give sincere thanks to Jessica Lundquist for her guidance and expertise.
J. Lundquist was supported by NASA grant NNX17AL59G.

References

Armstrong, R., Chang, A., Rango, A., & Josberger, E. (1993). Snow depths and grain-size relationships with relevance for passive microwave studies. Annals of Glaciology, 17, 171-176. doi:10.3189/S0260305500012799

Chang, A., Foster, J., & Hall, D. (1987). Nimbus-7 SMMR Derived Global Snow Cover Parameters. Annals of Glaciology, 9, 39-44. doi:10.3189/S0260305500200736

Chang, A. T. C., Foster, J. L., Hall, D. K., Rango, A., & Hartline, B. K. (1982). Snow water equivalent estimation by microwave radiometry. Cold Regions Science and Technology, 5(3), 259–267. https://doi.org/10.1016/0165-232X(82)90019-2

Dietz, A. J., Kuenzer, C., Gessner, U., & Dech, S. (2012). Remote sensing of snow – a review of available methods. International Journal of Remote Sensing, 33(13), 4094–4134. https://doi.org/10.1080/01431161.2011.640964

Derksen, C., Walter Strapp, J., Walker, A., Lemnietyinen, J., Hallikainen, M., & Pulliainen, J. (2006). A comparison of airborne passive microwave brightness temperatures and snowpack properties across the boreal forests of Finland and Western Canada. In International Geoscience and Remote Sensing Symposium (IGARSS) (pp. 694–697). https://doi.org/10.1109/IGARSS.2006.182

Durand, M., & Margulis, S. A. (2006). Feasibility Test of Multifrequency Radiometric Data Assimilation to Estimate Snow Water Equivalent. *J. Hydrometeor.* (2006) **7** (3): 443–457. https://doi.org/10.1175/JHM502.1

Durand, M., & Margulis, S. A. (2007). Correcting first-order errors in snow water equivalent estimates using a multifrequency, multiscale radiometric data assimilation scheme. Journal of Geophysical Research Atmospheres, 112(13), n/a-n/a. https://doi.org/10.1029/2006JD008067

Foster, J L, Chang, A. T. C., Hall, D. K., & Rango, A. (1991). Derivation of Snow Water Equivalent in Boreal Forests Using Microwave Radiometry (Vol. 44).

Foster, James L., Sun, C., Walker, J. P., Kelly, R., Chang, A., Dong, J., & Powell, H. (2005). Quantifying the uncertainty in passive microwave snow water equivalent observations. Remote Sensing of Environment, 94(2), 187–203. https://doi.org/10.1016/j.rse.2004.09.012

Hall, D. K., Foster, J. L., Chang, A. T. C., & Chung, A. T. C. (1982). Measurement and Modeling of Microwave Emission from Forested Snowfields in Michigan (Vol. 13). Retrieved from https://iwaponline.com/hr/article-pdf/13/3/129/9395/129.pdf

Hall, D. K., Foster, J. L., Verbyla, " D L, Klein, A. G., & Bensont, C. S. (1998). Assessment of Snow-Cover Mapping Accuracy in a Variety of Vegetation-Cover Densities in Central Alaska. REMOTE SENS. ENVIRON (Vol. 66). Elsevier Science Inc.

Kelly, R., Chang, A., Tsang, L., and Foster, J.L. (2003) . A prototype AMSR-E global snow area and snow depth algorithm". IEEE Transactions on Geoscience and Remote Sensing, vol. 41, no. 2, pp. 230-242.

Kim, R., Durand, M., Li, D., Baldo, E., Marguilis, S., Dumont, M., Morin, S. (2019). Estimating alpine snow depth by combining multifrequency passive radiance observations with ensemble snowpack modeling. Remote Sensing of Environment. 226, 1-15. https://dx.doi.org/10.1016/j.rse.2019.03.016

Langlois, A., Royer, A., Dupont, F., Roy, A., Goita, K. and Picard, G. "Improved Corrections of Forest Effects on Passive Microwave Satellite Remote Sensing of Snow Over Boreal and Subarctic Regions," in IEEE Transactions on Geoscience and Remote Sensing, vol. 49, no. 10, pp. 3824-3837, Oct. 2011.

Li, D., Durand, M., & Margulis, S. A. (2017). Estimating snow water equivalent in a Sierra Nevada watershed via spaceborne radiance data assimilation. Water Resources Research, 53(1), 647–671. https://doi.org/10.1002/2016WR018878

Larue, F., Royer, A., De Sève, D., Langlois, A., Roy, A., & Brucker, L. (2017). Validation of GlobSnow-2 snow water equivalent over Eastern Canada. Remote Sensing of Environment, 194, 264–277. https://doi.org/10.1016/j.rse.2017.03.027

Li, Q., Kelly, R., Leppanen, L., Vehvilainen, J., Kontu, A., Lemmetyinen, J., & Pulliainen, J. (2019). The Influence of Thermal Properties and Canopy-Intercepted Snow on Passive Microwave Transmissivity of a Scots Pine. IEEE Transactions on Geoscience and Remote Sensing, 57(8), 5424–5433. https://doi.org/10.1109/TGRS.2019.2899345

Long, D. G., & Brodzik, M. J. (2016). Optimum Image Formation for Spaceborne Microwave Radiometer Products. IEEE TRANSACTIONS ON GEOSCIENCE AND REMOTE SENSING, 54(5). https://doi.org/10.1109/TGRS.2015.2505677

Ly, V., Wrzensien, M., Vuyovich, C., Durand, M., Pestana, S., Lundquist, J. (2020) The pre-release Snow Sensor Usability Masks. http://doi.org/10.5281/zenodo.3994980.

Pulliainen, J. Mapping of snow water equivalent and snow depth in boreal and sub-arctic zones by assimilating space-borne microwave radiometer data and ground-based observations. *Remote Sensing of Environment* 2006, *101*, 257 - 269. https://doi.org/10.1016/j.rse.2006.01.002

Robinson, D., Dewey, K., & Heim, J. (1993), Global snow cover monitoring: An update, Bull. Am. Meteorol. Soc., 74, 1689–1696, doi:10.1175/1520-0477(1993)074<1689:GSCMAU>2.0.CO;2

Sturm, M., T. Grenfell, and D. Perovich, 1993. Passive microwave measurements of tundra and taiga snow covers in Alaska, U.S.A. Ann Glaciol, 17, 125-130.

Sturm, M., Holmgren, J., Liston, G. E., Sturm, M., Holmgren, J., & Liston, G. E. (1995). A Seasonal Snow Cover Classification System for Local to Global Applications. Journal of Climate, 8(5), 1261–1283. https://doi.org/10.1175/1520-0442(1995)008<1261:ASSCCS>2.0.CO;2

Takala, M. ; Luojus, K. ; Pulliainen, J. ; Derksen, C. ; Lemmetyinen, J. ; Karna, J. - P. ; Koskinen, J. ; Bojkov, B. Estimating northern hemisphere snow water equivalent for climate research through assimilation of space-borne radiometer data and ground-based measurements. *Remote Sensing of Environment* 2011, *115*, 3517 - 3529. https://doi.org/10.1016/j.rse.2011.08.014

Tedesco, M., Kim, E. J., England, A. W., De Roo, R. D., & Hardy, J. P. (2006). Brightness Temperatures of Snow Melting/Refreezing Cycles: Observations and Modeling Using a Multilayer Dense Medium Theory-Based Model. IEEE TRANSACTIONS ON GEOSCIENCE AND REMOTE SENSING, 44(12), 3563. https://doi.org/10.1109/TGRS.2006.881759

Robinson, D., K. Dewey, and R. Heim (1993), Global snow cover monitoring: An update, Bull. Am. Meteorol. Soc., 74, 1689–1696, doi:10.1175/1520-0477(1993)074<1689:GSCMAU>2.0.CO;2

Vander Jagt, B. J., Durand, M. T., Margulis, S. A., Kim, E. J., & Molotch, N. P. (2013). The effect of spatial variability on the sensitivity of passive microwave measurements to snow water equivalent. Remote Sens. Environ. 136(C), 163-179. https://doi.org/10.1016/j.rse.2013.05.002

Vander Jagt, B. J., Durand, M. T., Margulis, S. A., Kim, E. J., & Molotch, N. P. (2015). On the characterization of vegetation transmissivity using LAI for application in passive microwave remote sensing of snowpack. Remote Sensing of Environment, 156, 310–321. https://doi.org/10.1016/j.rse.2014.09.001

Varhola, A. and N, Coops. (2013). Estimation of watershed-level distributed forest structure metrics relevant to hydrologic modeling using LiDAR and Landsat. Journal of Hydrology. 70(86), 487. DOI: 10.1016/j.jhydrol.2013.02.032

Vuyovich, C. M., Jacobs, J. M., & Daly, S. F. (2014). Comparison of passive microwave and modeled estimates of total watershed SWE in the continental United States. Water Resources Research, 50(11), 9088–9102. https://doi.org/10.1002/2013WR014734

Appendix

Appendix 1. Data Pre-processing. All datasets were upscaled to 25km pixel resolution and reprojected to WGS 84.

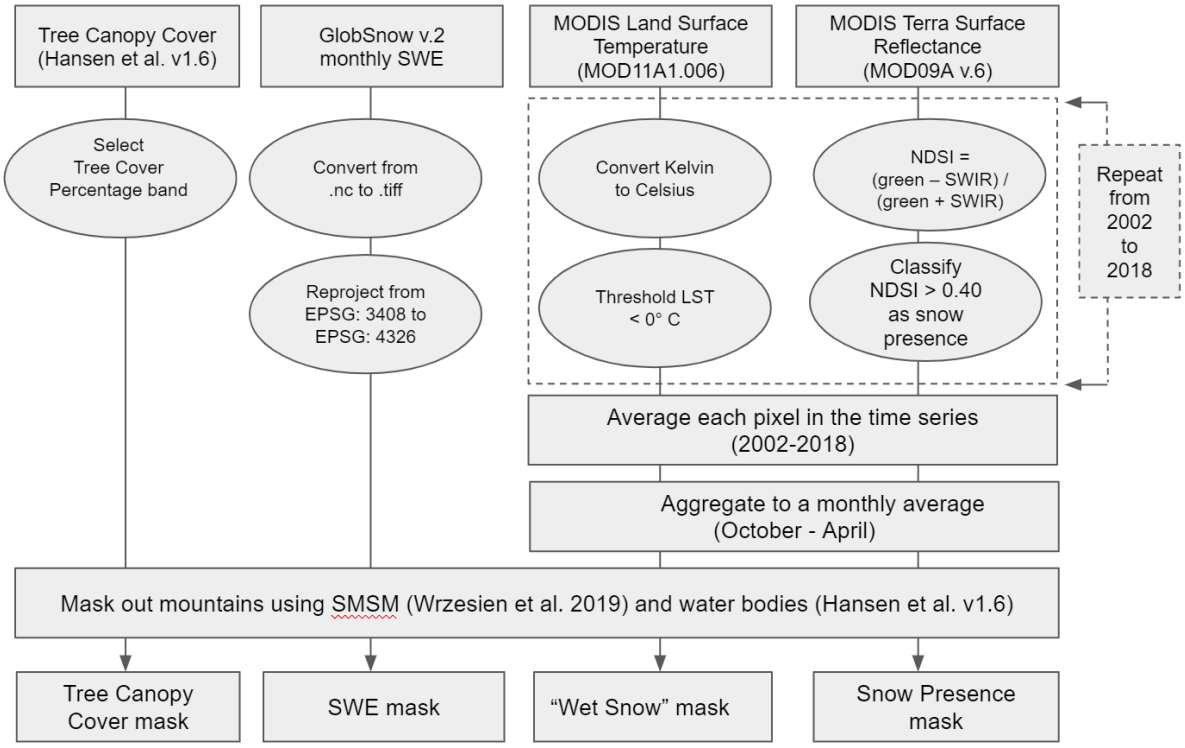

Appendix 2. Summary Statistics for input SWE datasets: NoahMP ECMWF, NoahMP GDAS, and GlobSnow SWE [mm] for Quebec, Canada. N is the number of pixels in each dataset. P10 and p90 are the 10th and 90th percentiles. In order to match the resolution of NoahMP SWE datasets and in-situ observations, Globsnow SWE was resampled to 5km. Globsnow SWE was processed from 1979-2016. NoahMP SWE was processed from 2009-2017.

Dataset	N	Mean	Std. deviation	Min	p10	Median	p90	Max
NoahMP ECWMF	50250	173.4	43.8	104.7	122.9	162.5	236.7	442.2
NoahMP GDAS	73637	213.7	40.4	83.0	161.9	208.8	268.2	534.8
GlobSnow	76488	98.3	25.5	3.0	68.6	97.3	132	167.8